Physical modeling of the densification of snow/firn and ice in the upper part of polar ice sheets

Laurent Arnaud, Jean M. Barnola and Paul Duval

Laboratoire de Glaciologie et de Géophysique de l'Environnement, CNRS, B.P. 96, 38402 St. Martin d'Hères Cedex, FRANCE

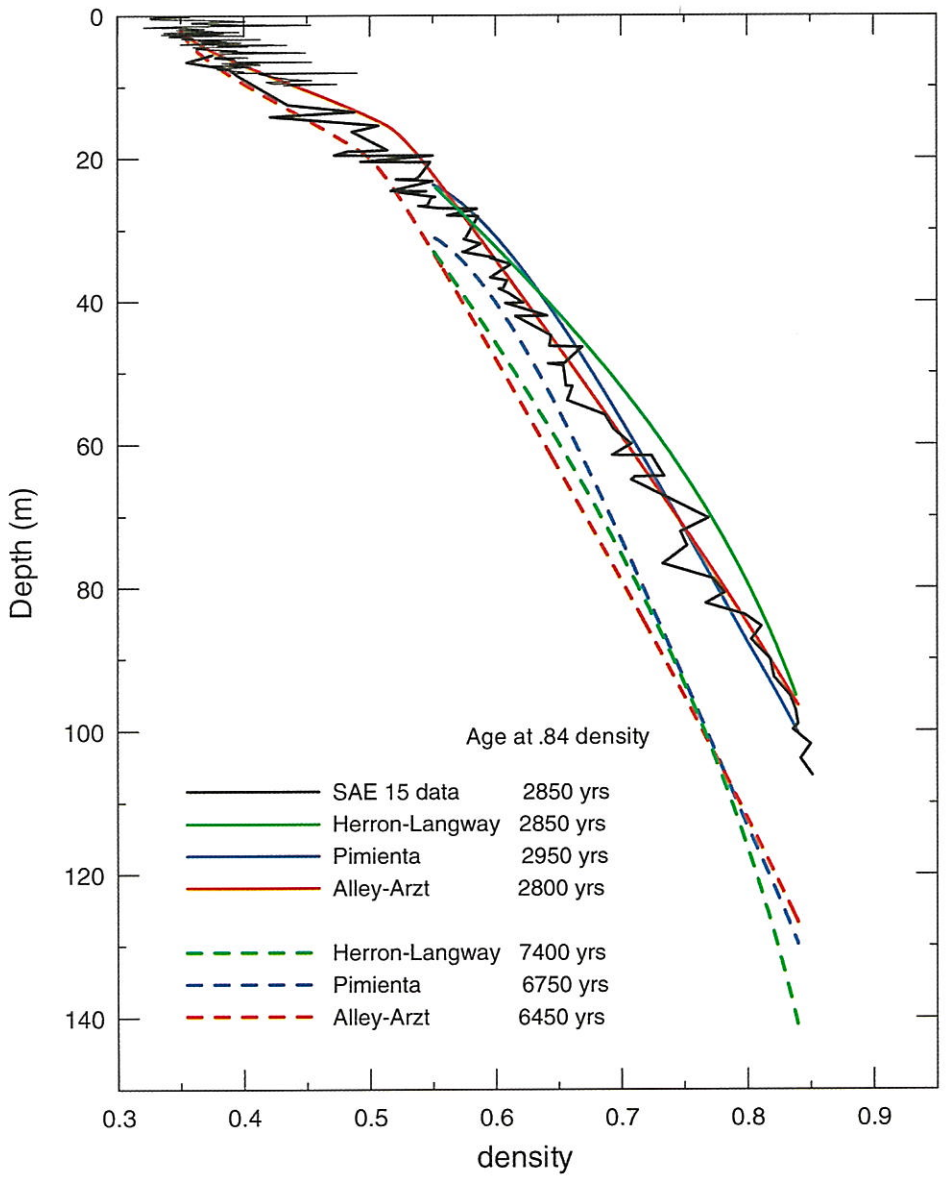

Plate 8. L. Arnaud et al., Figure 3.

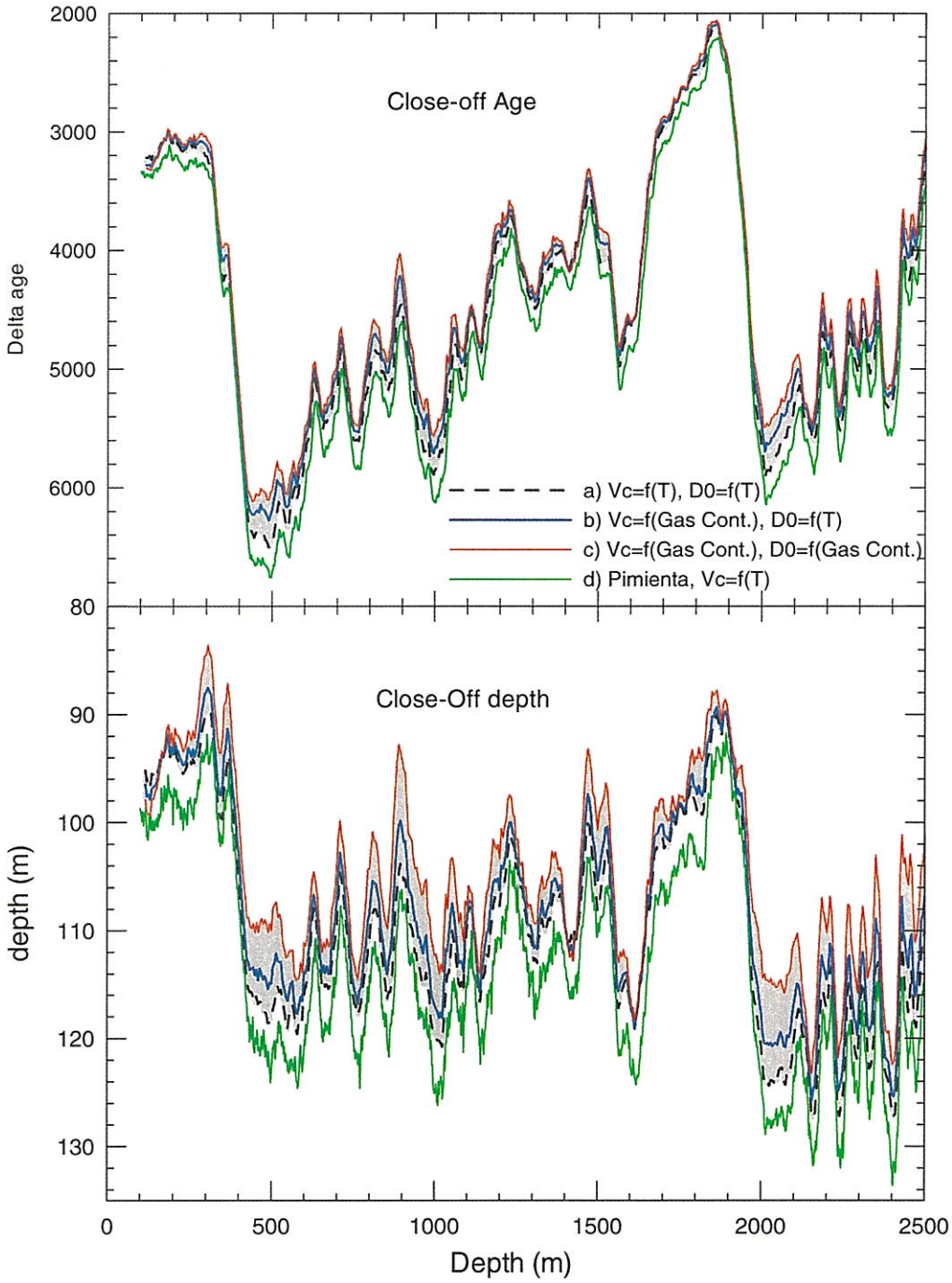

Plate 9. L. Arnaud et al., Figure 7.

Physical modeling of the densification of snow/firn and ice in the upper part of polar ice sheets

Laurent Arnaud, Jean M. Barnola and Paul Duval

Laboratoire de Glaciologie et de Géophysique de l'Environnement, CNRS, B.P. 96, 38402 St. Martin d'Hères Cedex, FRANCE

Abstract: We propose a model for the densification of snow, firn, and ice that includes the following: the densification of isothermal snow by grain boundary sliding [Alley, 1987], the microscopic approach of Arzt [1982] for the geometrical description of porous materials during densification, and plastic deformation with a power law creep for firn and ice densification. Current density profiles are well reproduced by this physical model assuming variations of the relative density at the snow-firn transition. This density, D_0, corresponds to the change from densification by deformationless restacking to densification by power law creep.

D_0 is always lower than the theoretical packing density for mono-sized spheres (D_0 = 0.64) and decreases with temperature; its low values are unlikely to be an effect of the particle size distribution, but instead arise from nonuniform densification. Variations of D_0 with temperature are correlated with variations of the load between sites for a given density. D_0 could also be modified by differences in porosity structure during snow metamorphism due to different surface conditions (for instance, wind, surface temperatures, and temperature gradients).

Applied to past climatic conditions of Vostok, Antarctica, the densification model predicts close-off ages and depths during the last climatic cycles. Through variations of D_0 parameters, uncertainties in these predictions were estimated.

1. Introduction

Environmental information preserved in polar ice is associated either with the ice matrix, for instance the temperature which depends on the isotopic content of the ice; or it is associated with the air trapped in the ice, as is the atmospheric composition. Because the air is trapped at the firn-ice transition (the close-off depth, approximately 80 m below the surface), to link the information in the air to that in the ice it is crucial to know precisely the conditions that snow transforms into ice. The following are needed: (a) the close-off density, (b) the age of the gas at this density, (c) the age of the ice, and (d) the close-off depth.

(a) The close-off density can be estimated from measurements of the evolution of closed porosity on firn samples [Schwander et al., 1984, 1993; Kameda

Physics of Ice Core Records
Edited by T. Hondoh
Hokkaido University Press, 2000, Sapporo

and Naruse, 1994]. However, these measurements were from small samples that need corrections to get the effective close-off density. Another way is to measure the total gas content of the ice; then, when the atmospheric pressure and the temperature are known, it allows to estimate the density at which the air is isolated from the atmosphere (in terms of pressure) [Martinerie et al., 1992]. This method has been applied to a large number of different firns, and an empirical relationship between the firn temperature (present-day climate) and the pore volume V_i when the air is isolated has been found:

$$V_i(\mathrm{cm^3/g}) = 7.6\times10^{-4}T(\mathrm{K}) - 0.057. \quad (1)$$

However, gas content profiles of the Vostok core suggests that this empirical relationship might not be valid for all the past climatic conditions, and also that wind could affect the pore volume at the isolation depth [Martinerie et al., 1994].

(b) The age of the air in the firn, and thus at the close-off depth, has been studied by diffusion models validated by measurements of the composition of interstitial firn air. The gravitational separation of different elements that causes an enrichment of the heavier compounds as a function of firn depth were included. This allows one to reproduce the concentrations of atmospheric compounds measured in the firn air [Schwander et al., 1993; Trudinger et al., 1997], and also to reconstruct their atmospheric history using an inverse method [Rommelaere et al., 1997]. These models showed that the air is few tens of years old at the base of the firn, and their age range can smooth the concentration of the trapped gas over a few centuries when the accumulation rate is very low (as it is at Vostok).

(c) The age of the ice at the close-off is the main parameter to link the ice and gas records. When no density measurements are available, densification models have to be used as discussed below.

(d) The close-off depth can be estimated by measuring the gravitational enrichment of ^{15}N of N_2 trapped in air inclusions [Sowers et al., 1992], or it can be estimated using firn-densification models.

When no data are available, the precision of the last two parameters depends on quality of the firn-densification model. Furthermore, recent studies use independent information to determine the air dating or trapping depths, and then use a densification model to get climatic information. For instance, Schwander et al. [1997], working on the GRIP core, used CH_4 to get a gas chronology for GRIP and ^{15}N to get close-off depths, and then ran a densification model with different climatic parameters to fit the data and thus calibrate the glacial to interglacial temperature change in Greenland. Similarly, the Greenland CH_4 records of GISP or GRIP, which are of global significance, are now widely used to synchronize Antarctic and Greenland ice cores through densification models [Blunier et al., 1998; Steig et al., 1998]. These examples show that firn-densification models should both reproduce the present- day situations and predict firn profiles under climatic conditions having no present-time analogues. The Vostok total gas content profile [Martinerie et al., 1994] shows that an empirical relationship based

on present-day data might not be valid for the past. This stresses the need for a physical model instead of an empirical one. We present a physical model based on pressure sintering and apply it to past Vostok climatic conditions.

2. Densification model

The formation of ice in polar ice sheets results from the densification of dry snow and firn. This densification is similar to the hot pressing procedure in ceramics and metals in which pressure is applied during sintering at high temperature, except that on ice sheets the pressure is due to the accumulation of snow at the surface.

Three stages of densification are generally distinguished. During the first stage, the densification of snow is mainly a structural rearrangement of grains by grain-boundary sliding. Sintering is driven by the temperature gradient in the first few meters and by surface tension. Transport mechanisms such as evaporation-condensation and surface diffusion contribute to rounding of the grains and to intergranular bonding [Benson, 1962; Gow, 1975]. The rearrangement of unbounded grains dominates the densification of highly porous snow. Alley [1987] proposed a first model for densification by grain boundary sliding for snow below 2-m depth where temperature-gradient effects are unimportant. From Anderson and Benson [1963], this particle rearrangement is complete at a critical density of about 0.55 g/cm^3, corresponding to a relative density of 0.6, which can be regarded as the maximum packing density. Moreover, according to Benson [1962] and Arnaud [1997], this critical density increases with temperature, and the depth at which this density is reached increases as the temperature decreases [Anderson and Benson, 1963; Gow, 1975; Herron and Langway, 1980]: at −57 °C it is approximately 30 m [Alley, 1980] and at −23 °C it is approximately 12 m [Herron and Langway, 1980]. In addition to the dependence on temperature, the accumulation rate for a given temperature can also affect the depth of the critical density [Herron and Langway, 1980; Nishimura et al., 1983]

The second stage is firn (consolidated snow). Because seasonal variations of surface temperature disappear, the transformation of firn into ice can be considered as isothermal. The end of this stage is characterized by the growth of the impermeable pore space fraction under the increasing overburden pressure. The average number of bonds per grain (coordination number) increases with density from approximately 6 at the start of this stage to 16 for ice [Gow, 1969, this work]. Plastic deformation increases this coordination number and causes neck growth; particle motion is negligible.

During the final stage, atmospheric air is trapped in cylindrical or spherical pores; further densification of this bubbly ice is driven by the pressure lag between the ice matrix and the air in bubbles [Maeno and Ebinuma, 1983; Pimienta, 1987; Alley and Bentley, 1988; Salamatin et al., 1997].

Numerous empirical models describing the densification of snow, firn and ice that fit experimental density profiles have been developed [Bader, 1962; Anderson and Benson, 1963; Kojima, 1964; Herron and Langway, 1980; Kameda et al., 1994]. They were established and validated with depth-density data from many sites in Greenland and Antarctica.

In the last few years there was a major advance in our understanding of the mechanisms which contribute to densification during hot-powder compaction. Hot-isostatic pressing maps were made for various materials. Dominant mechanisms of densification were identified and densification rates were calculated as a function of pressure, temperature and powder characteristics [Ashby, 1990]. It was shown that for the densification of firn and ice, power-law creep is the controlling mechanism in the second stage and for the first part of the final stage [Maeno and Ebinuma, 1983; Arzt et al., 1983; Ebinuma and Maeno, 1987; Wilkinson, 1988]. Newtonian creep becomes the dominant densification mechanism of bubbly ice as soon as the effective pressure, defined as the difference between the ice pressure and the pressure within bubbles, becomes lower than 0.3 MPa [Pimienta and Duval, 1987; Lipenkov et al., 1997]. Concerning structural evolution during the second stage of densification, the Wilkinson and Ashby [1975] model assumed a constant size and number of contact per particles and spherical pores which are questionable assumptions [Swinkels et al., 1983]. This problem was partially solved for polar ice studies by Barnola et al. [1991] by introducing an empirical function into the Wilkinson and Ashby model that includes all structural variations during densification. However, the physical meaning of this function is not clear, and the extrapolation to other past climatic conditions (e.g., climatic or glacial transitions) might not be valid.

A microscopic approach for the geometrical theory of pressure sintering of mono-sized spherical powders that includes the continuous formation of particle contacts and the growth of the average contact area was developed by Arzt [1982] and Fischmeister and Arzt [1983]. The continuous increase in coordination is modeled by assuming a random dense-sphere packing of monosized spheres with a radial distribution function [Scott, 1962; Mason, 1968]. Densification is modeled by allowing each (spherical) particle to increase in radius around fixed centers. As each particle grows, both the number of bonds per grain and the average area per contact increase. The coordination number Z_0 for a random dense packing of spheres equals 7.3 with D_0 (the relative density) equals 0.64. At D_0 the area of each contact is assumed to be zero. For the final stage with closed pores, densification is determined by the creep of the thick shell surrounding each hole [Wilkinson and Ashby, 1975].

One purpose of this work is to validate the approach proposed by Arzt [1982] for simulating the depth-density profiles of firn and ice in polar ice sheets. This model is used with the snow densification model of Alley [1987] to describe densification in the entire upper part of polar ice sheets. This physical densification model helps to understand how the initial snow structure and climate causes differences of firn densification between sites. In the last section, this model is used to reconstruct past density profiles.

2.1 Density profiles in polar snow, firn and bubbly ice

We will focus the analysis of densification profiles on two Antarctica sites: Byrd [Gow, 1968] and Vostok [Barkov, 1973]. The main characteristics of these sites are given in Table 1 and their density profiles are plotted in Fig. 1a. For a

Table 1: Main characteristics of the studied sites in Antarctica and Greenland.

	De08	Site 2	D47	Byrd	Dome C	Vostok
Mean Surface Temperature (°c)	-19°c	-23.3°c	-25.4°c	-28°c	-54°c	-57°c
Accumulation rate (Mg m^{-2} yr^{-1})	1.1	0.41	0.25	0.16	0.034	0.022
Load pressure at 0.55 Mg m^{-3} (MPa)	0.035	0.06	0.05	0.063	0.109	0.123
Location	66° 43' S 113° 11' E	76° 59' N 56° 04' W	67° 23' S 138° 43' E	79° 59' S 120° 01' W	74° 30' S 123° 10' E	78° 28' S 106° 48' E
References	(Etheridge and Wookey, 1989)	(Langway, 1967)	(Arnaud and others, 1998)	(Gow, 1968)	(Alley, 1980)	(Barkov, 1973)

given density, the overburden pressure is higher at Vostok station than at Byrd. Table 1 shows similar results for other sites; for a given density of 0.55 g/cm^3, the overburden pressure is higher at the colder sites.

The effect of the accumulation rate is shown in Fig. 1b, which gives the relationship between the density and the age of ice. At Vostok, the transition from firn to ice, corresponding to the end of the pore closure process, was observed for a density of about 0.84 g/cm^3. The age of the ice at this transition is around 2800 years. At Byrd, the firn to ice transition is observed for a density of 0.825 g/cm^3 and the age of ice is only 250 years [Barnola et al., 1991].

2.2 Equations governing densification of isothermal snow

Although the snow metamorphism at the surface due to temperature gradients or mechanical effects (wind) must cause some differences of densification between sites (formation of the initial structure of the material before densification), this study is limited on densification modeling. Then, the densification model starts at the 2-m depth, the shallowest depth where temperature gradient effects become unimportant [Alley, 1987]. The densification of isothermal snow is mainly a structural rearrangement of grains by grain boundary sliding. Alley [1987] proposed a first physical model for densification by grain boundary sliding. To be consistent with the firn densification model (which has one parameter), the model of Alley has been slightly modified to have also only one parameter. (See §2.4 for the snow to firn transition.)

The densification rate given by Alley [1987] for grain boundary sliding can be written,

$$dD/dt = \gamma (A/D^2)(1 - (5/3)D)t\,, \qquad (2)$$

where $\gamma = R/(vr^2)$. R and r are the grain and the bond radii, respectively, and can be assumed constant during this first stage of densification. The parameter γ includes all constant quantities: the viscosity of the grain boundaries v (assuming isothermal conditions), and the geometrical parameters R and r. The constant γ is set such that the densification rate is continuous at the

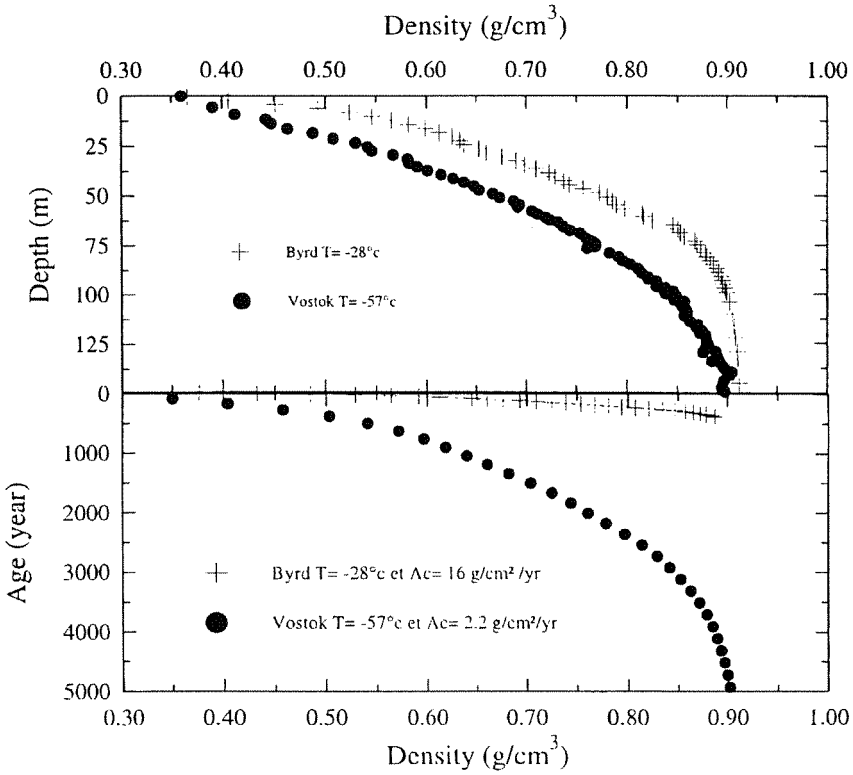

Figure 1: Depth-density (1.a) and time-density (1.b) profiles for two sites: Vostok and Byrd.

transition between snow and firn (see §2.3 and 2.4).

2.3 Equations governing densification of firn and bubbly ice

When grain sliding becomes negligible in the model, the densification rates are obtained by assuming that power-law creep is the densification mechanism. The constitutive equation is:

$$\dot{\varepsilon} = A\sigma^n, \qquad (3)$$

where $\dot{\varepsilon}$ and σ are the equivalent strain rate and stress, respectively. A and n are the creep constant and the stress exponent, respectively.

Second stage: firn (0.6 < D < 0.9)

Equations for the densification rate of firn of initial density D_0 are directly derived from the geometrical model developed by Arzt [1982]. This rate is:

$$dD/dt = 5.3A(D^2D_0)^{1/3}(a/\pi)^{1/2}(P^*/3)^n, \qquad (4)$$

where $P^* = 4\pi P/aZD$, a is the average contact area in units of R^2 (R is the initial particle radius), P equals the ice load pressure, P^* is the real pressure acting on an average contact area, and Z the coordination number at the relative density D. The driving force due to surface tension is always very low compared to that resulting from the external pressure [Gow, 1968]: for a typical pore radius of 0.1 mm, the pressure due to the surface tension is

about 1 kPa (i.e., very low compared to the ice pressure).

The stress exponent n of the flow law is assumed to be 3 [Ebinuma and Maeno, 1987]. The temperature dependence of the creep constant A is Arrhenius; we assumed

$$A(T) = 7.89\times10^{3}\exp(-Q/RT)\,,$$

where Q, the activation energy, was deduced from the densification of bubbly ice [Pimienta, 1987], to equal 60 kJ·mol^{-1}. R and T are the gas constant and the absolute temperature, respectively.

We could not use the approximation proposed by Helle et al. [1985] because it predicts $Z_0 = 7.7$ with $D_0 = 0.64$ and $Z = 12$ when full density is reached; whereas in our case, the relative density at maximum packing was always less than 0.64 and likely dependent on temperature [Benson, 1962; this study]. Therefore, we used the more complete equations of Fischmeister and Arzt [1983] to calculate variations of Z and a versus D (see Appendix). To obtain the initial coordination number Z_0 for various values of D_0, we assumed that P^* approaches P as D tends towards 1.

Final stage: bubbly ice (0.9 < D < 1)

At the bottom part of the firn, the open pores begin to be isolated and can be assimilated to cylinders. Just below the close-off depth, the effective pressure is greater than 0.3 MPa [Lipenkov et al., 1997]; consequently, the stress exponent can be assumed to be 3 [Duval and Castelnau, 1995]. The densification rate is given by the deformation of ice shells surrounding cylinders [Wilkinson and Ashby, 1975]:

$$dD/dt = 2A\left\{D(1-D)/\left[1-(1-D)^{1/n}\right]^{n}\right\}\left(2P_{eff}/n\right)^{n}. \quad (5)$$

The effective pressure, P_{eff}, now equals $P - P_b$, where P_b is the pressure in the bubbles. This pressure is calculated from the conditions at the close-off (i.e., relative density D_c and atmospheric pressure P_c) and the Boyle-Mariotte equation:

$$P_b = P_c\{D(1-D_c)/[D_c(1-D)]\}$$

As the density increase, the ratio of the cylindrical to spherical bubble number decreases continuously. At Vostok station (East Antarctica), cylindrical bubbles are observed down to 150 m (Fig. 4). Also, the pressure in the bubbles increases and the effective pressure decreases with depth. Consequently, densification can be modeled as deformation of spherical pores during the last part of the final stage (D>0.95), and because the stress will become lower than 0.3 MPa, the stress exponent of the flow law equals 1 [Pimienta and Duval, 1987]. Thus, the densification rate becomes

$$dD/dt = (9/4)A(1-D)P_{eff}\,. \quad (6)$$

During the transition from $n = 3$ to $n = 1$ (or cylindrical to spherical pores), the model calculates the two densification rates and uses the more rapid one.

Comparison with experimental data

From equations (4), (5) and (6), the densification rate can be expressed as a function of the effective pressure as follows:

$$dD/dt = A\cdot f(D)\cdot P_{eff}^{n}\,. \quad (7)$$

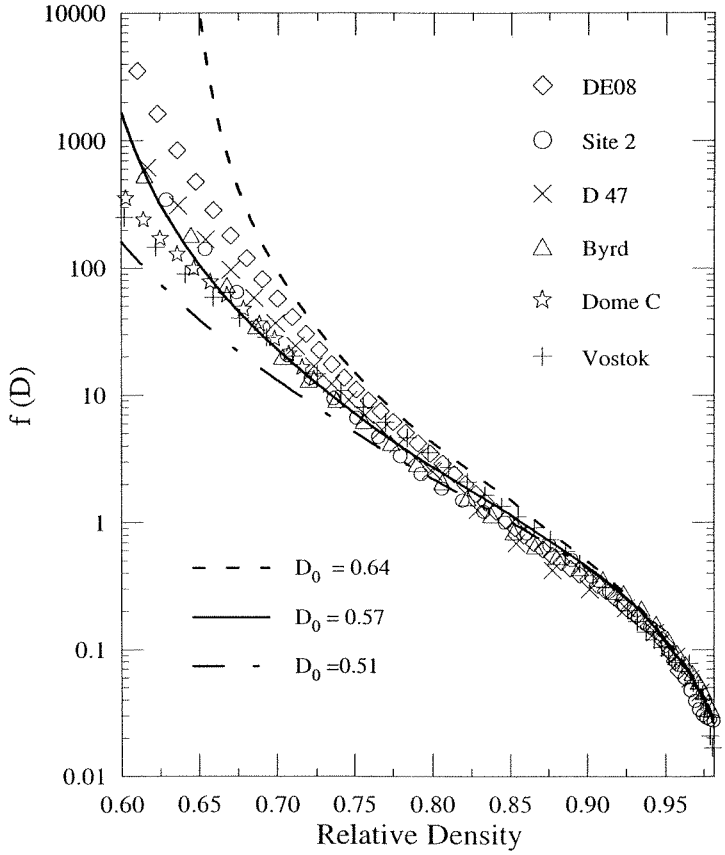

Figure 2: Experimental function f versus relative density for six sites from Greenland and Antarctica (Table 1). The theoretical curves giving the variation of $f(D)$ with density were obtained for three values of D_0.

The experimental values of $f(D)$ were calculated from equation (7) and densification profiles of several sites in Antarctica and Greenland (c.f. Table 1). Equations (4), (5) and (6) for firn and bubbly ice were used to model the variation of $f(D)$ (Fig. 2).

The experimental data (Fig. 2) agree fairly well with the predictions of the theory of densification behavior of Fischmeister and Arzt [1983] and Wilkinson and Ashby [1975]. However, there are small deviations from the theoretical curve at the beginning of the second stage. Furthermore, the initial density D_0 that best fits the experimental data is lower than that for the random, dense-packing of mono-sized spheres (0.64). As shown in Fig. 2, variations of D_0 between 0.51 and 0.64 are necessary to reproduce the densification profiles of firn between –19 °C to –57 °C and D_0 appears to decrease with temperature.

Density-depth profiles simulated for Vostok present-day and glacial conditions with the empirical model from Herron Langway [1980], the semi-empirical model of Pimienta [Barnola et al., 1991] and the geometrical model (this work) are compared in Fig. 3. For the present-day conditions, the best agreement with the

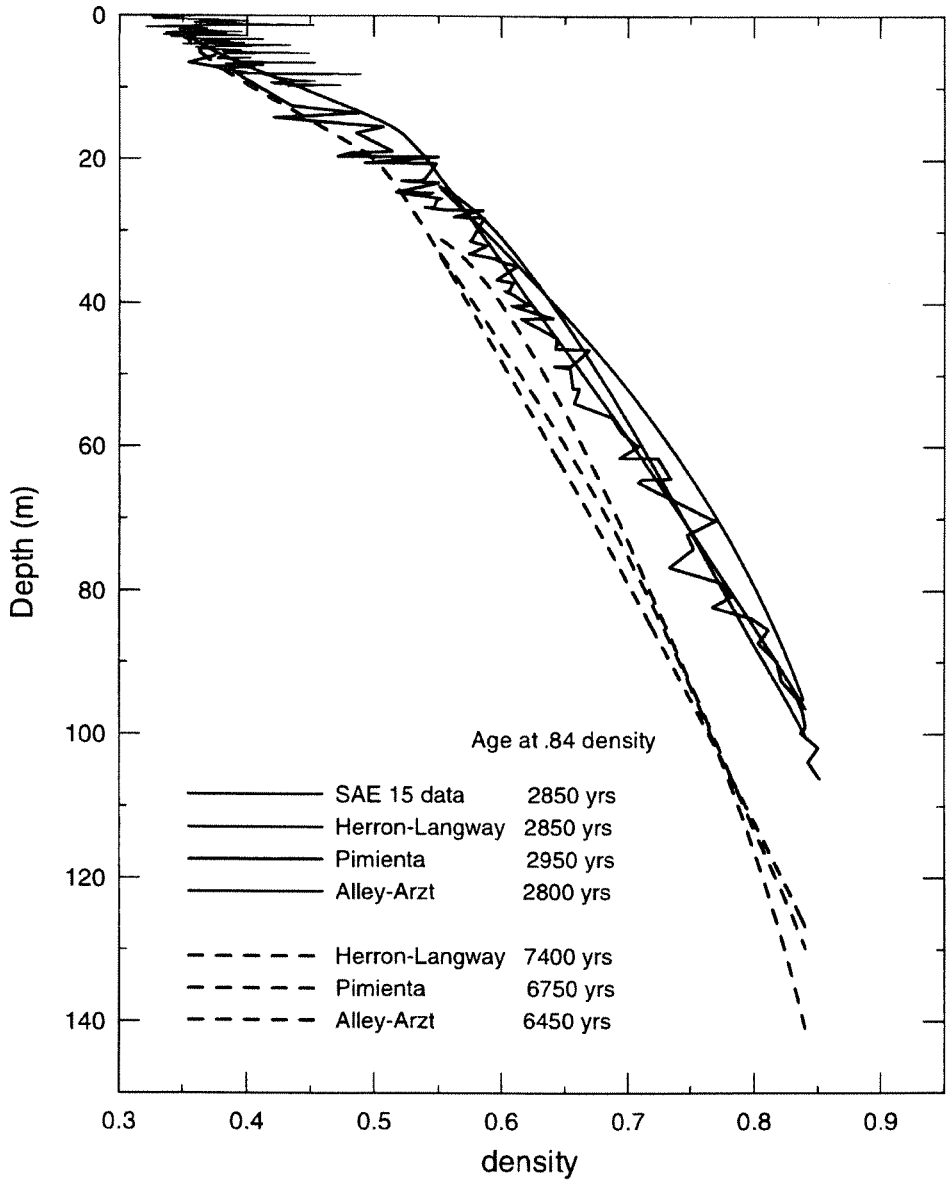

Figure 3: Density profiles simulated by different models for present-day (continuous lines) and glacial conditions (dotted lines) compared to the field SAE 15 data [Barkov, 1973]. (See color plate 8.)

measured profile [Barkov, 1973] is obtained by the geometrical model with D_0 = 0.53. However, at the density of 0.84, the three models predict similar depths and ages for the present-day conditions, although this is not the case when the simulations are done with conditions of the last glacial maximum (T = –67 °C and a_c = 1.25 g/cm^{2}yr). For the latter conditions, which have no present equivalent, the depth of the 0.84 density varies from 140 m with the empirical approach of Herron and Langway to 127 m with the geometrical model. These correspond to ages of ice

ranging from 7400 years to 6450 years. The difference between predictions from the Pimienta and the geometrical models comes mainly from the choice of D_0; in the former, D_0 is fixed at 0.57, but in the latter it varies with temperature.

2.4 Structure of snow, firn and ice

An advantage of the geometrical model is the possibility of linking densification to the structure of the material to understand the influence that climate parameters have on densification processes at the surface of the ice sheet.

The technique used to characterize the structure of snow, firn, and ice is based on photographs of polished surfaces of thick samples using reflected light [Arnaud et al., 1998a]. This new observation method simul-taneously allows the determination of the porous network and grain boundaries from a single image. As a second step, image processing of these photographs allowed determination of the parameters defined above [Arnaud, 1997; Gay, 1999]. Figure 4 shows the evolution of the porous

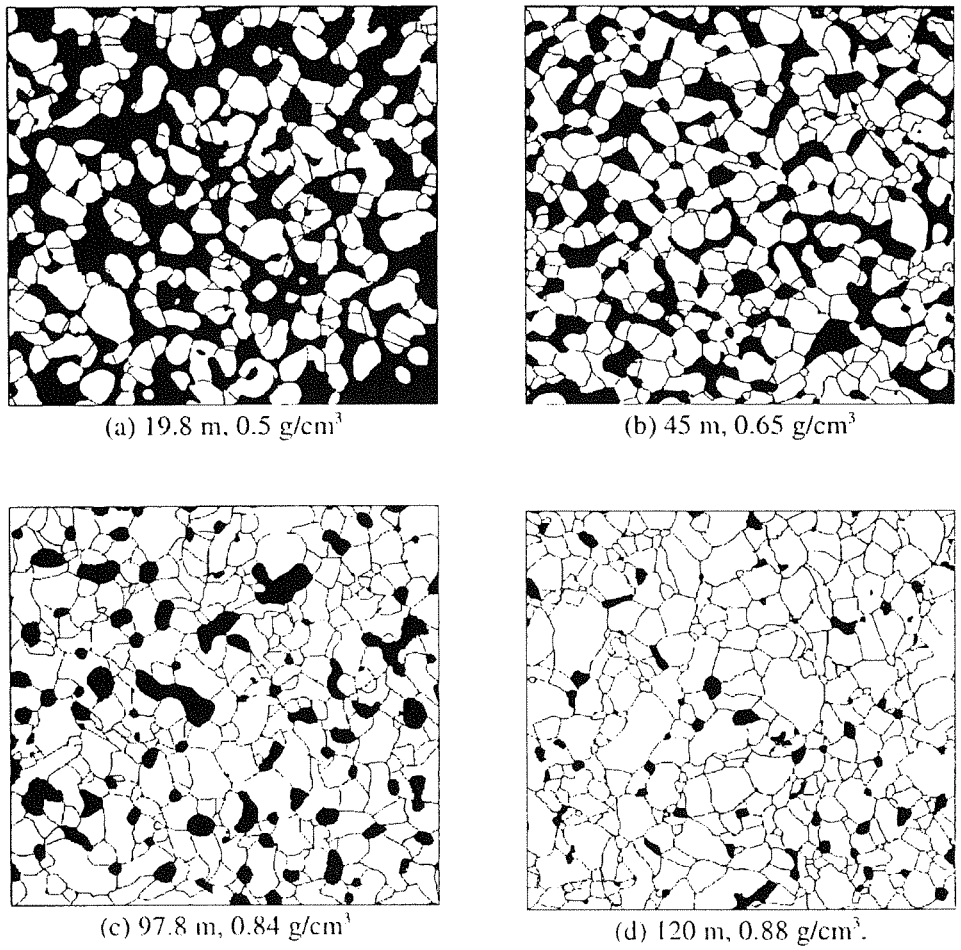

Figure 4: Binary images obtained by image processing of photographs obtained in reflected light from sections of the Vostok core. (a) 19.8 m, 0.5 g/cm^3; (b) 45m, 0.65 g/cm^3; (c) 97.8 m, 0.84 g/cm^3; (d) 120 m 0.88 g/cm^3.

structure from snow to ice in the Vostok ice core.

Variations of packing density within a compact powder are common; low density regions containing large pores can develop during the early stage of sintering as a result of nonuniform densification. The non-uniform structure of firn is illustrated in Fig. 4. The average contact area between ice crystals is significant at the theoretical initial density D_0. Some grains without any contact with pore can be seen in the two-dimensional structure of firn in Fig. 4.

In addition to these qualitative observations, a quantitative validation of the geometrical densification model of Arzt was obtained from this structural characterization of polar firn [Arnaud et al., 1998b]. The parameters necessary to test densification models include the average number of bonds per grain (Z) and the average contact area relative to the grain size (a). These parameters cannot be calculated directly with two-dimensional structural analysis. Therefore, a different structural parameter was chosen for this study: the surface fraction of the average grain involved in grain bonds (β). This parameter is also known as the contiguity factor [Underwood, 1970], and can be determined using two-dimensional analysis. In this case, β is related to the specific surface area of the grain-pore interface (S_v(g-p)) and the specific surface area of the grain boundary (S_v(g-g)):

$$\beta = 2S_v(\text{g-g})/[2S_v(\text{g-g}) + S_v(\text{g-p})] .$$

From the model structural parameters (Z and a), β is given by:

$$\beta = Za/4\pi .$$

The change in the average fraction of the surface area of grains involved in bonds (β) with density at Vostok (Fig. 5) agrees with data obtained by Alley and Bentley [1988] and complements the direct observations shown in Fig. 4. More than 40 % of the surface area of grains is involved in grain boundaries at the relative density of 0.6, whereas the theoretical value must equal zero at the beginning of the firn densification.

Snow grains are generally composed of polycrystalline ice grains and this texture is retained during the metamorphism [Fuchs, 1959; Sommerfeld and La Chapelle, 1970; Arons and Colbeck, 1995]. The formation of grain bonds during the densification of snow could result from its structure either at deposition time or just after the metamorphism in the top few meters depth. In fact an explanation for the presence of grain bonds at the stage of snow compaction is plastic deformation of ice grains under the overburden pressure. Both deformation and grain boundary sliding would occur concurrently at the beginning of compaction. There will certainly be small regions where particle rearrangement without deformation is prevalent, but also other regions where flat areas form by plastic deformation. Thus, the transition from snow to firn corresponds to a change in the dominant densification mechanism. Particle rearrangement by sliding is the dominant densification mechanism in snow, and power-law creep is the dominant one in firn, but both mechanisms must operate in a density range close to the transition D_0. The physical meaning of the initial density D_0 is described in more detail by Arnaud et al. [1998b].

Figure 5 also suggests that the particle in the geometrical densification model of

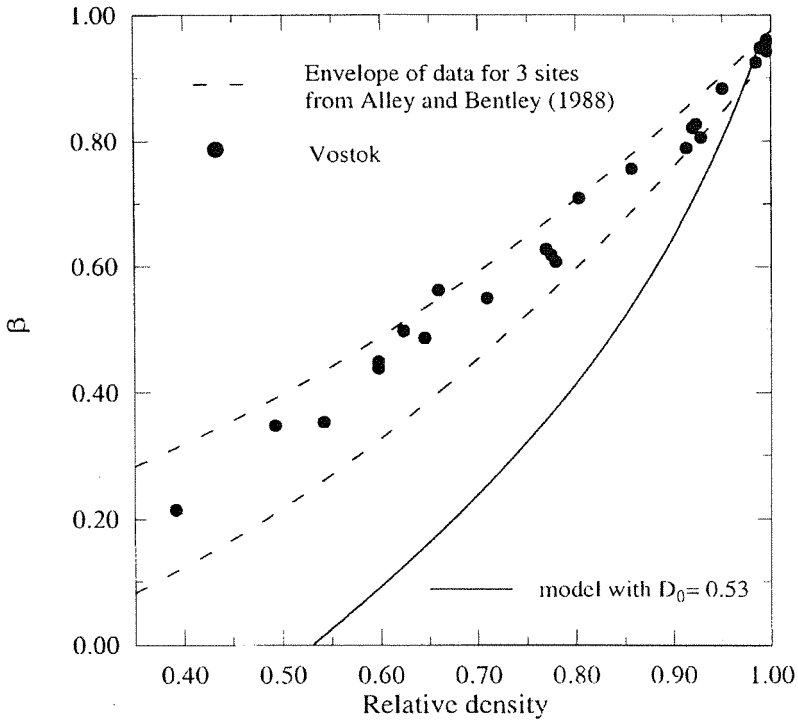

Figure 5: Average fraction of the surface of crystals involved in bonds (β) for Vostok, and envelopes of the data from three other sites from Alley and Bentley [1988]. Model curves with $D_0 = 0.53$.

Arzt [1982] should contain more than one grain. From the success of this densification model for describing firn (Fig. 2), we have assumed that at D_0 the particle is not a grain, but an aggregate of grains to make the contact area between aggregates equal zero at D_0. This is physically compatible with the occurrence of power-law creep during the densification of snow, even if this densification mechanism (power-law creep) is not yet dominant.

Assuming that densification by plastic deformation involves groups of crystals (aggregates), not single grains, the parameter β_a for the aggregate must equal zero at D_0. S_{v0}(g-p) is the specific surface area of the grain-pore interface at D_0; this value also equals the specific surface area of the aggregate-pore interface. Assuming a constant average surface area of aggregates, the parameter $(1 - \beta_a)$, which represents the fraction of free surface area of the average aggregate, is

$$1 - \beta_a = S_v(\text{g-p})/S_{v0}(\text{g-p}) .$$

In Fig. 6, the dependence of this parameter on relative density is compared with that obtained by assuming there is no aggregate. These structural data are also compared with model curves. The results, shown in Fig. 6, are compatible with a description of the firn as a group of aggregates. Moreover, the structural evolution observed during densification is well reproduced by the geometrical model of Arzt.

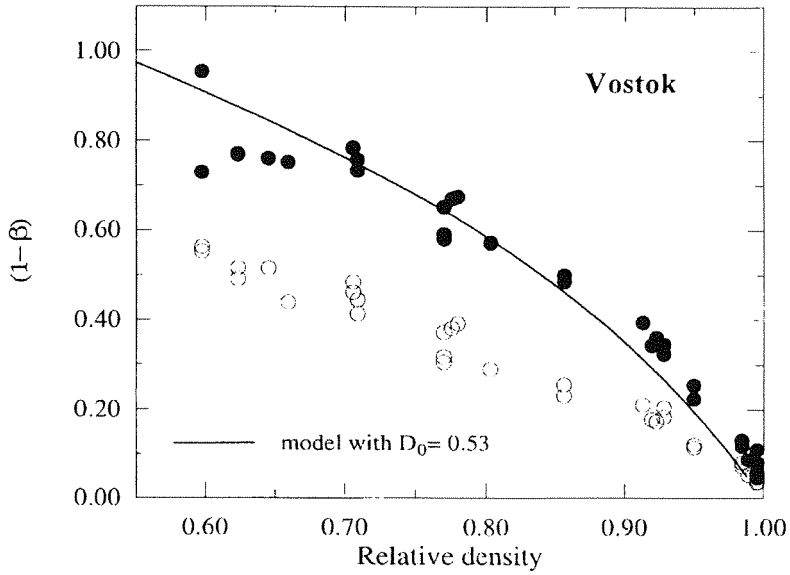

Figure 6: Fraction of free surface area of grain (●) and aggregate (○) versus relative density for Vostok (Bh7). Model curves with $D_0 = 0.53$.

2.5 The snow-firn transition: D_0

The value of D_0 = 0.64, deduced assuming a random dense-packing of mono-sized spheres for the initial particle structure, is probably too high for polar firn. The distribution of particle sizes and shapes affects the parameters D_0 and Z_0 [Bouvard and Lafer, 1990]; for instance, D_0 should be larger with spherical particles of different sizes [Aparicio and Cocks, 1995]. With the model of Artz, densification by power-law creep is supposed to occur as soon as the dense packing of spheres is reached. The packing density D_0 that best fits the model corresponds to the end of grain-boundary sliding as the significant densification mechanism. As a result, the theoretical maximum packing density cannot be reached.

The observed variation of D_0 with location would also result from the competition between grain boundary sliding and power-law creep. The comparison of density profiles as a function of depth shows that the depth where the relative density equals 0.6 increases as the mean annual temperature of the site decreases [Nishimura et al., 1983]. For a 40 °C decrease of the mean annual temperature (i.e., the difference between Vostok and De08 sites), the overburden pressure corresponding to the relative density of 0.6 is multiplied by about 4 (Table 1). This change is well reproduced by the model of densification by grain boundary sliding established by Alley [1987] for the first stage of densification. Grain-boundary sliding is proportional to stress (Newtonian process), which contrasts with the flow law exponent of 3 for particle deformation. Thus, concerning the effect of pressure, the density D_0 at the transition between the first and the second stage should decrease with temperature. Hence, power law creep should prevail at a lower density in cold sites. Probably, this effect partly causes the

decrease of D_0 with site temperature. But, it is also necessary to include the variation of ice viscosity with temperature. The activation energy for the grain boundary viscosity is about 42 kJ·mol^{-1} [Alley, 1987], and about 60 kJ·mol^{-1} for the power-law creep. The variation of the activation energy with densification processes therefore partially counteracts the load effect. In support of this, including both the effects of load and temperature, Arnaud et al. [1998b] showed that in the cold site the power law creep process becomes the dominant densification mechanism at lower density. The final effect is a decrease with temperature of the relative density D_0, corresponding to the transition between snow and firn. This agrees with the results in Fig. 2. Moreover, Benson [1962], who directly measured the "critical density" between the densification stages, observed a range of values from 0.62 to 0.56 for the temperature range from –16 °C to –30 °C. From the available data [Arnaud, 1997], D_0 could be related to the temperature by:

$$D_0 = 0.00226T\,(\mathrm{K}) + 0.03\,. \qquad (8)$$

This relationship is empirical; thus as for the close-off density, it could have been different in the past. Also, Arnaud [1997] proposed that the structure of the material at this density influences the structural properties of the firn, particularly those determining the close-off porosity. In this case, the empirical relationship between this last parameter and the temperature (equation (1)) would come from the physical relation between D_0 and T, and we should have:

$$V_c = 0.319D_0 - 0.059. \qquad (9)$$

3. Reconstruction of the past density profiles

A common application of a densification model is to determine the difference between the age of ice and that of the gas, and the close-off depths during the past to compare the information trapped in the bubbles to those linked with the ice. Thus we have to extrapolate the empirical links between temperature and close-off density or critical density to previous periods.

In Fig. 7 are plotted the age of the ice and the close-off depth as reconstructed for the first 2500 m of the Vostok core. (This includes the last two glacial-interglacial climatic cycles.) Results from the densification model of Pimienta and from our geometrical model with different assumptions are shown. For all cases, the temperatures and accumulation rates are those adopted for the GT4 chronology [Petit et al., 1999]. Calculations were made in a Lagragian reference, and the temperature perturbations were assumed to propagate rapidly through the firn layers. For the geometrical model, we assumed the following for cases a) – c):

a) D_0 varies with temperature following equation (8), and the close-off density changes according to equation (1).
b) D_0 varies with temperature following equation (1), and the close-off density follows the total gas content changes from Martinerie et al. [1994]. In this case, we assumed that equation (1) was not valid during the past and that all changes in the total gas content recorded in the Vostok core were due to changes in the close-off density. (Similarly, to explain the Vostok gas content profile, Martinerie et al. [1994]

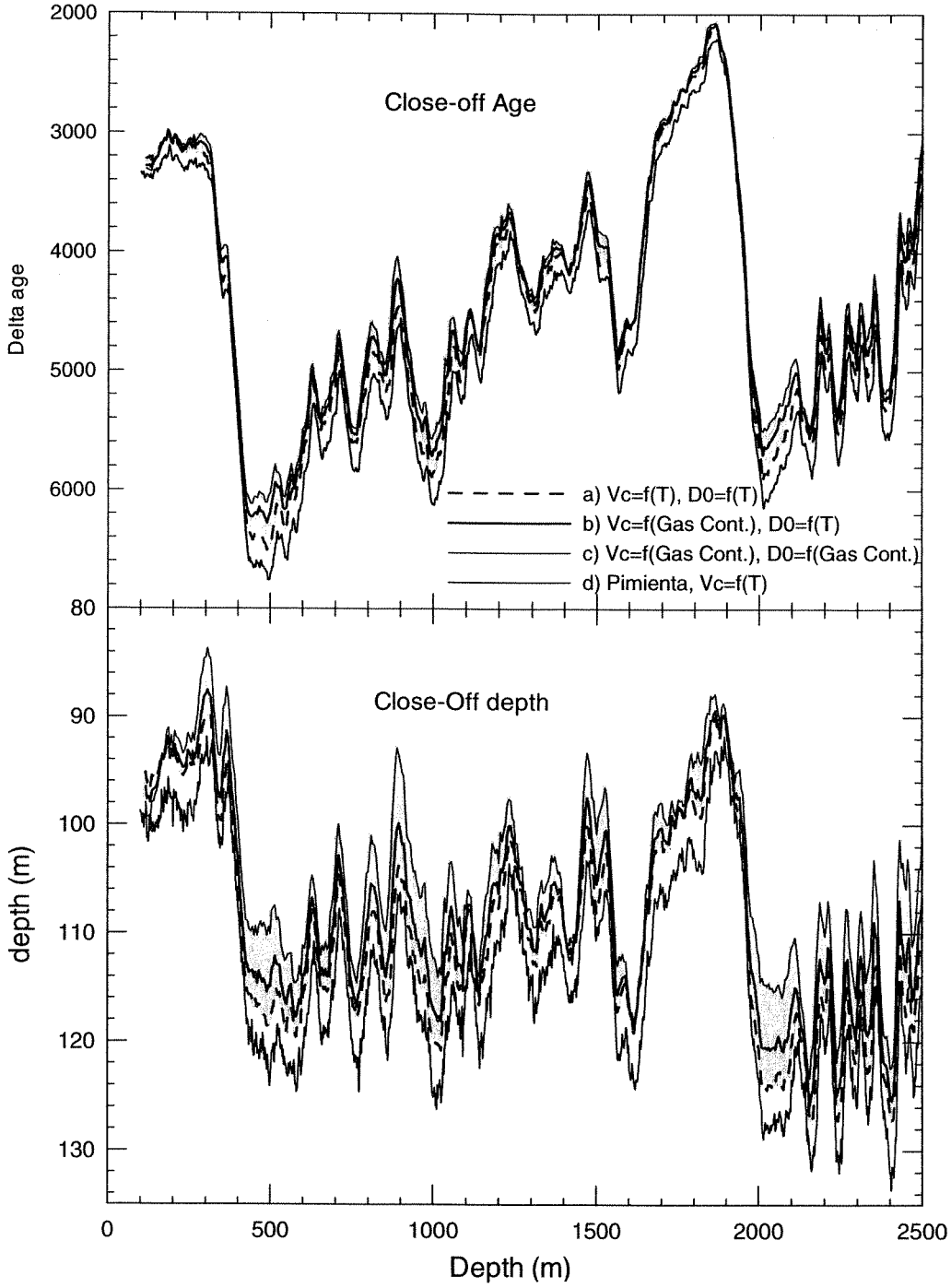

Figure 7: Close-off age (upper panel) and depth (lower panel) reconstructed for the first 2500m of the Vostok core. a, b and c curves correspond to different assumptions in the geometrical model (see text) and d to the Pimienta model. (See color plate 9.)

evoked a change in altitude and in the temperature-close-off density relationship.) However, for a sensitivity test we assumed that the atmospheric pressure remained constant during the past 220,000 years, even though this is unlikely.

c) D_0 and the close-off density follow the gas content changes with D_0 linked to the close-off density by the equation (9). In this case, we assumed that equation (8) also was not valid in the past.

The age of the ice at the close-off follows pretty well the climatic variations and varies between 2000 and 3000 years during the interglacial periods (0 to 300-m and 1650 to 1900-m depths) up to 6750 years during the coldest periods. Without additional constraints, it is difficult to decipher between the different cases; thus, the maximum uncertainty in the close-off age determination is about 650 years (during the full glacial periods), and is always less than 10 % of the close-off age. However, we argue that the geometrical model is better suited than the Pimienta model for predicting close-off ages under different climatic conditions. In this case, the age from our model is about 400 years younger during the coldest periods than that previously assumed, and the associated uncertainty, taken as the shaded area in Fig. 7, is slightly less than 10 %.

The close-off depths also follow the climatic variations. However, with the assumption in the geometrical model that D_0 and V_c follow the gas content changes (case c), the close-off depth during some cold periods (around 900 m and 1500 m) can be as shallow as those during warm periods. Also, while the age increases by a factor of two between interglacial and glacial periods, the depth change is only about 25 %; similarly, the depth variations between the different assumptions are also relatively large. Therefore, it appears that the close-off depths are relatively less constrained than the close-off ages.

One advantage of the geometrical model for comparing gas and ice information is that it predicts uncertainties in the close-off ages and depths of about 10 %. To reduce this value it will be necessary to better understand the influence of climate on D_0, V_c, and more generally, on the firn structure. In this context, the development of tools to get independent estimates of close-off ages and depths are very promising. For example, Nitrogen and Argon isotopic measurements allow, through the thermal diffusivity, comparison of the same temperature signal both in ice and in bubbles, and thus can indicate the firn thickness [Severinghaus et al., 1998].

Conclusion

We constructed a physical densification model of snow, firn, and ice on the basis of grain sliding in the first stage and then by plastic deformation and structural evolution of a porous material in later stages. Differences in initial firn structures are included through the density of the snow-firn transition, D_0. Empirically, this density depends on temperature for which we propose an explanation. We have also suggested a link between this density and the close-off density, and reconstructed past close-off depths and ages for the Vostok core. However, the development of new measurements to recover past structural parameters, or new tracers based on isotopic gas composition are needed to

assess the validity of the empirical relationships based on present conditions.

Appendix

Average contact area (a) and coordination number (Z) versus relative density (D)

The modeling of the particle geometry and calculations are from Arzt [1982] and Fischmeister and Arzt [1983]. Powder particles are assumed spherical with the same radius, and the initial geometry approximates that of random dense packing. The treatment of homogeneous densification is easier if, instead of letting the center-to-center distances shrink, we let the particles grow around their fixed centers.

The new particle radius R' (in units of the initial particle radius R) after this fictitious growth is

$$R'(D) = (D/D_0)^{1/3}. \qquad \text{(A-1)}$$

After growth to this new radius, some particles overlap. The number of these overlaps is calculated using the radial density function (RDF) for random, dense-packing [Scott, 1962; Mason, 1968]. The average number of sphere centers located within radius $r = 2R'$ from the reference sphere is equal to the average coordination number Z:

$$Z(D) = G(2R') = Z_0 + C(R' - 1), \qquad \text{(A-2)}$$

where $G(r)$ integrated radial density function.

Moreover, the overlap produces an excess volume of material that is distributed uniformly over those parts of the sphere surfaces that are not in the contacts. S_0, the new mean radius of the truncated sphere R'' (in units of the initial particle radius R) is calculated from this excess volume assuming mass conservation. It is

$$R'' = R' + \frac{[4Z_0(R'-1)^2(2R'+1)+c(R'-1)^3(3R'+1)]}{[12R'\{4R'-2Z_0(R'-1)-c(R'-1)^2\}]}. \qquad \text{(A-3)}$$

The average contact area a (in unit of R^2) is obtained by averaging over all existing contacts: Z_0 contacts of maximum size, plus some progressively smaller ones. This average area is

$$a(D) = a(R'') = (\pi/3ZR'^2)\left[3(R''^2-1)Z_0 + R''^2 c(2R''-3)+c\right]. \qquad \text{(A-4)}$$

Acknowledgements

This work was supported by the Programme National d'Etude de la Dynamique du Climat (PNEDC), CNRS, and by Environment Program of the Commission of European Communities (CEC). We acknowledge the Russian Antarctic Expeditions, the Division of Polar Programs of the US National Science Foundation (NSF), and IFRTP for their logistic support at Vostok station. We thank A. Manouvrier for the ice drilling and M. Gay for the image processing.

References

Alley, R.B. 1980. Densification and re-crystallization of firn at Dome C, East Antarctica. *Institute of Polar Studies Report* **77**.

Alley, R.B. 1987. Firn densification by grain boundary sliding: a first model. *J. Phys.* (Paris), **48-C1**, 249-256.

Alley, R.B. and Bentley C. R. 1988. Ice-core analysis on the Siple coast of west Antarctica. *Ann. Glaciol.*, **11**, 1-7.

Anderson, D.L. and Benson C.S. 1963. The densification and diagenesis of snow. *Ice and Snow, the MIT Press,* W. D. Kingery, Ed., 391-411.

Aparicio, N.D. and Cocks A.C.F. 1995. On the representation of random packing of spheres for sintering simulations. *Acta metall. mater.*, **43**, 3873-3884.

Arnaud, L. 1997. Modélisation de la transformation de la neige en glace à la surface des calottes polaires; Etude du transport des gaz dans ces milieux poreux. *Thèse de Doctorat de l'Université Joseph Fourier de Grenoble (Phd).*

Arnaud, L., Gay M., Barnola J.M., and Duval P. 1998a. Imaging of firn and bubbly ice in coaxial reflected light : a new technique for the characterization of these porous media. *J. Glaciol.*, **44**, 326-332.

Arnaud, L., Lipenkov V.Ya., Barnola J.M., Gay M. and Duval P. 1998b. Modeling of the densification of polar firn : characterization of the snow-firn transition. *Ann. Glaciol.*, **26**, 39-44.

Arons, E.M. and Colbeck S.C. 1995. Geometry of heat and mass transfer in dry snow: a review of theory and experiment. *Reviews of Geophysics,* **33**, 463-493.

Arzt, E. 1982. The influence of an increasing particle coordination on the densification of spherical powders. *Acta Metall.* **30**, 1883-1890.

Arzt, E., Ashby M.F. and Easterling K. E. 1983. Practical applications of hot-isostatic pressing diagrams: four case studies. *Metallurgical Trans. A*, **14**, 211-221.

Ashby, M.F. 1990. *Software for constructing maps for sintering and isostatic pressing diagrams: HIP 6.0, and operating manual.* Cambridge, University Engineering Department.

Bader, H. 1962. Theory of densification of dry snow on high polar glaciers II. *CRREL Res. Rep.*, **108**. (published in Kingery, 1960, 351-376)

Barnola, J.M., Pimienta P., Raynaud D., and Korotkevich Y.S. 1991. CO_2-climate relationship as deduced from the Vostok ice core: a re-examination based on new measurements and on a re-evaluation of the air dating. *Tellus*, **43** (B), 83-90.

Barkov, N.I. 1973. Rezultaty issledovaniia skvazhiny i ledianogo kerna na stantsii Vostok v 1970-1972 [Results of the investigation of borehole and ice core research at Vostok Station 1970-1972] *Materialy Glyatsiologicheskikh Issledonaniy. Khronika. Obsuzhdeniya* **22**, 77-81.

Benson, C.S. 1962. Stratigraphic Studies in the Snow and Firn of the Greenland Ice Sheet. *SIPRE Res. Rep.*, **70**, 76-83.

Blunier T., Chgappellaz J., Schwander J., Dällenbach A., Stauffer B., Stocker T.F., Raynaud D., Jouzel J., Clausen H.B.,

Hammer C.U. and Johnsen S.J. 1998. Asynchrony of Antarctic and Greenland climate change during the last glacial period. *Nature*, **394**, 739-743.

Bouvard D. and Lafer M. 1990. New developments in modeling of hot isostatic pressing taking into account size distribution and contact interactions. *in Proc. 2nd Int. Conf. on Hot Isostatic Pressing, Gaithersburg, Maryland, American Society of Metals* edited by R.J Schaefer and M. Linzer.

Duval P. and Castelnau P. 1995. Simulations of anisotropy and fabric development in Polar ice. *J. Phys.* (Paris) **5-C3,** 197-205.

Ebinuma T. and Maeno N. 1987. Particle-rearrangement and dislocation-creep in a snow densification process. *J. Phys.* (Paris), **48-C1**, 263-270.

Etheridge, D.M. and Wookey C.W. 1988. Ice core drilling at a high accumulation area of law dome, Antarctica *in Proc. of the III Int. Workshop on ice core drilling technology, Grenoble, oct. 1988 in Ice Core Drilling.*

Fischmeister, H.F. and Arzt E. 1983. Densification of powders by particle deformation. *Powder Metallurgy,* **26**, 82-88.

Fuchs, A. 1959. Some structural properties of Greenland snow. *S.I.P.R.E. Res. Rep.*, **42**, 1-24.

Gay, M. 1999. Caractérisation de la neige, du névé et de glace par traitement d'images. *Thése de doctorat de l'Université Joseph Fourier de Grenoble (Phd).*

Gow, A.J. 1968. Deep core studies of the accumulation and densification of snow at Byrd Station and Little America V, Antarctica. *U.S. CRREL Res. Rep.* **197**.

Gow, A.J. 1969. On the rates of growth of grains and crystals in South Polar firn. *J. Glaciol.*, **8**, 241-252.

Gow, A.J. 1975. Time-temperature dependence of sintering in perennial isothermal snowpacks. Symposium on Snow Mechanics, Grindelwald, avril 1974. *A.I.H.S. Publication* **114**, 25-41.

Helle A.S., Easterling K.E. and Ashby M.F. 1985. Hot isostatic pressing diagrams: New developments. *Acta Metall.* **33**, 2163.

Herron, M.M. and Langway C.C. 1980. Firn densification: an empirical model. *J. Glaciol.*, **25**, 373-385.

Kameda T., Shoji H., Kawada, K., Watanabe O. and Clausen H.K. 1994. An empirical relation between overburden pressure and firn density. *Ann. Glaciol.*, **20**, 87-94.

Kameda T. and Naruse R. 1994. Characteristics of bubble volumes in firn-ice transition layers of ice cores from polar ice sheets. *Ann. Glaciol.*, **20**, 95-100.

Kojima, K. 1964. Densification of snow in Antarctica. *Antarct. Res. Ser.*, **2**, 157-218.

Langway, C.C. 1967. Stratigraphic analysis of a deep ice core from Greenland. *CRREL Res. Rep.* **77**.

Lipenkov, V.Ya., Salamatin A.N. and Duval P. 1997. Bubbly ice densification in ice sheets: II. Applications. *J. Glaciol.*, **43**, 397-407.

Maeno, N. and Ebinuma T. 1983. Pressure sintering of ice and its implication to the

densification of snow at polar glaciers and ice sheets. *J. Phys. Chem.*, **87**, 4103-4110.

Martinerie P., Raynaud D., Ethridge D.M., Barnola J.M. and Mazaudier D. 1992. Physical and climatic parameters which influence the air content in polar ice. *Earth Planet. Sci. Lett.*, **112**, 1-13.

Martinerie P., Lipenkov V.Ya., Raynaud D., Chappellaz J., Barkov N.Y. and Lorius C. 1994. Air content paleo record in the Vostok ice core (Antarctica): A mixed record of climatic and glaciological parameters. *J. Geophys. Res.*, **99**, 10565-10576.

Mason, G. 1968. Radial distribution functions from small packing of spheres. *Nature*, **217**, 733-735.

Nishimura, H., Maeno N. and Satow K. 1983. Initial stage of densification of snow in Mizuho Plateau, Antarctica. *Mem. Nat. Inst. Polar Res. Spec. Issue*, **29**, 149-154.

Petit, J.R. and others 1999. Climate and atmospheric history of the past 420,000 years from the Vostok ice core, Antarctica. *Nature*, **399**, 429-436.

Pimienta, P. 1987. Etude du comportement mécanique des glaces polycristallines aux faibles contraintes; applications aux glaces des calottes polaires. *Thèse de Doctorat de l'Université Joseph Fourier de Grenoble.*

Pimienta, P. and Duval P. 1987. Rate controlling processes in the creep of polar glacier ice. Proc. of the VII Int. Symposium on the Physics and Chemistry of Ice. *J. Phys.(Paris)*, **48-C1**, 243-248.

Rommalaere V., Arnaud L. and Barnola J.M. 1997. Reconstructing recent atmospheric trace gas concentrations from polar firn and bubbly ice data by inverse methods. *J. Geophys. Res.*, **102**, 30069-30083.

Salamatin, A.N., Lipenkov V.Ya. and Duval P. 1997. Bubbly ice densification in ice sheets: I. Theory. *J. Glaciol.*, **43**, 387-396.

Schwander J. and Stauffer B. 1984. Age difference between polar ice and the air trapped in its bubbles. *Nature*, **311**, 45-47.

Schwander J., Barnola J.M., Andrié C., Leuenberger M., Ludin A., Raynaud D. And Stauffer B. 1993. The age of the air in the firn and the ice at Summit, Greenland. *J. Geophys. Res.*, **98**, 2831-2838.

Schwander J., Sowers T., Barnola J.M., Blunier T., Fuchs A. and Malaizé B. 1997. Age scale of the air in the Summit ice: Implication for glacial-interglacial temperature change. *J. Geophys. Res.*, **102**, 19483-19493.

Scott, G.D. 1962. Radial distribution of random close packing of equal spheres. *Nature*, **194**, 956-957.

Severinghaus J.P., Sowers T., Brook E.J., Alley R.B. and Bender M.L. 1998. Timing of abrupt climate change at the end of the Younger Dryas interval from thermally fractionated gases in polar ice. *Nature*, **391**, 141-146.

Sommerfeld, R.A. and La Chapelle E. 1970. The classification of snow metamorphism. *J. Glaciol.*, **9**, 3-17.

Sowers T., Bender M., Raynaud D. and Korotkevich Y.S. 1992. $*^{15}N$ of N_2 in air trapped in polar ice: a tracer of gas transport in the firn and a possible constraint on ice age-gas age differences. *J. Geophys. Res.*, **97**, 15683-15697.

Steig E.J., Brook E.J., White J.W.C., Sucher C.M., Bender M.L., Lehman S.J.,Morse D.L. Wadington E.D. and Clow G.D. 1998. Synchronous climate changes in Antarctica and the North Atlantic. *Science*, **282**, 92-95.

Swinkel, F.B., Wilkinson, D.S., Arzt, E. and Ashby, M.F. 1983. Mechanisms of hot isostatic pressing. *Acta Metall.*, **31**, 1829-1893.

Trudinger C.M., Enting I.G., Etheridge D.M., Francey R.J., Levchenko V.A., Steele L.P. Raynaud D. and Arnaud L. 1997. Modeling air movement and bubble trapping in firn. *J. Geophys. Res.*, **102**, 6747-6763.

Underwood, E.E. *ed.* 1970. *Quantitative Stereology*. Reading, MA, Addison-Wesley Publishing.

Wilkinson, D.S. 1988. A pressure- sintering model for the densification of polar firn and glacier ice. *J. Glaciol.*, **34**, 40-45.

Wilkinson, D.S. and Ashby M.F. 1975. Pressure sintering by power law creep. *Acta Metall.*, **23**, 1277-1285.